Enhancing Microgrid Resilience with Green Hydrogen Storage

Shreshtha Dhankar *Student Member, IEEE,*   Cong Chen *Student Member, IEEE,*   Lang Tong *Fellow, IEEE*

Abstract—We consider the problem of hydrogen storage integration in microgrids to improve the electricity supply resilience. Nonlinear effects from electrochemical models of electrolyzers and fuel cells for hydrogen storage are considered, making scheduling under the nonlinear model intractable and the conventional linear approximation infeasible. A piecewise linear model approximation with feasibility projection is proposed, resulting in a computationally efficient model predictive control for hydrogen storage operation. Several resilience performance measures, such as loss-of-load, duration-of-outage, and system cost, are used in performance evaluation. Simulations for the proposed optimization demonstrated a 13%-48% reduction in duration-of-outage, a 6.4%-21.7% reduction in system cost, and a 95% reduction in loss-of-load for critical loads compared to the scheduling algorithm involving linear model approximation. The performance gap of the proposed optimization to the benchmark involving the accurate nonlinear electrochemical model is less than 1% in most metrics.

Index Terms—Green hydrogen storage, resilience, electrochemical model, piecewise linear approximation, microgrid.

I. INTRODUCTION

The large-scale integration of intermittent renewable resources and the increasing occurrence of severe climate events pose significant challenges to the resilience of the modern power grid. It has been widely recognized that microgrids operating at both grid-connected and islanding modes are promising ways to reduce customer outages and enhance overall resilience. To this end, a synergistic operation of local renewable generation, storage charging/discharging, and prioritized scheduling of flexible demand is critical in minimizing the loss-of-load and outage duration.

This work focuses on the role of green hydrogen storage for microgrid resilience. Compared with electric battery systems, hydrogen storage is a strong candidate for long-duration energy storage owing to its high energy density and negligible self-discharge rate [1]. Surplus renewable can be harnessed by electrolyzers to produce green hydrogen. With advances in electrolyzer and fuel cell technologies and the economy of scale, green hydrogen is poised to be a dual-use technology critical to the economic and resilient operations of the decarbonized power and transportation systems. During events when power from the parent grid is lost or severely curtailed, the microgrid can convert green hydrogen back into electricity with fuel cells to enhance the system resilience.

Shreshtha Dhankar (sd728@cornell.edu) is with the School of Chemical Engineering, Cornell University, Ithaca NY, USA. Cong Chen and Lang Tong ({cc2662, lt35}@cornell.edu) are with the School of Electrical and Computer Engineering, Cornell University, Ithaca NY, USA. (Corresponding author: Cong Chen)

A. Summary of contribution

We develop novel modeling and optimization techniques to enhance microgrid resilience, taking into account the nonlinear electrochemical characteristics of electrolyzers and fuel cells.

First, we propose a resilience-enhancing energy management system (EMS) for a microgrid capable of operating at both grid-connected and islanding modes. The EMS optimizes the scheduling of prioritized demand, distributed energy resources (eg. roof-top solar), and electrolyzer and fuel cell operations under several objective functions involving loss-of-load norms as resilience metrics.

Second, we propose a piecewise linear approximation of the nonlinear electrochemical hydrogen storage model and a feasibility projection approach, resulting in a significantly reduced computation complexity. This makes it possible for the real-time operations of microgrid and hydrogen storage with a model predictive control (MPC) implementation.

Third, we present numerical simulation results, demonstrating performance gain over the assumed conventional linear hydrogen charging-discharging model. In particular, we show that the piecewise linear approximation resulted in less than 1% gaps in system cost and total loss-of-load when compared with the accurate but more expensive nonlinear model. Compared with the state-of-the-art linear model, on the other hand, the proposed piecewise linear approximation solution reduces duration-of-outage by 13%-48%, system cost by 6.4%-21.7%, and the loss-of-load by 95%.

Our simulation also provided insights into the effectiveness of different loss-of-load penalty functions used in the objective function. Specifically, we showed that the l_1-norm penalty function worked best in reducing total loss-of-load. The mixed norm (i.e., a weighted sum of l_1 and l_∞ norms) was preferred if both the maximum loss-of-load and the total loss-of-load were important resilience metrics. And l_2-norm penalty outperformed others in shortening the duration-of-outage.

B. Related work

The hydrogen storage model is critical to this resilience-enhancing EMS. We summarize three types of hydrogen storage models. Type I establishes a linear hydrogen storage model with constant charging/discharging efficiency [2], [3]. Such a linear model relies on the manufacturer's efficiency specifications or linear regression for power-hydrogen relationships. The model simplicity enables efficient real-time decisions in bulk system operation and control problems [2]. However, this approach tends to overlook the crucial electrochemical dynamics of hydrogen storage. Type II approximates the nonlinear electrochemical models of hydrogen storage with piecewise linear models [4], [5]. Such a method balances the

model's precision and computation burden. Type III directly employs nonlinear electrochemical models [6]–[9] to conduct simulations on device-level research for hydrogen storage. Such a model is too complicated to be included in a system-level optimization.

Our method belongs to Type II. We conduct piecewise linearization for power-hydrogen relationships of the hydrogen storage. Existing models in Type II usually characterize hydrogen by volumetric flow rate (m^3/s) [4]. But the dependence of gas volume on operating conditions (eg. temperature, and pressure)[1] poses challenges in monitoring hydrogen gas volume across the entire operation cycle including electrolyzers, storage tanks, and fuel cells. To address this, our approach considers *mass flow rate* (kg/s) as it offers a consistent measure for hydrogen, unaffected by variations in the operating conditions. Additionally, most hydrogen storage approximation methods [2]–[5] ignore the issue that they may produce infeasible dispatch signal resulted from approximation errors. We resolve this issue by proposing a real-time feasibility projection embedded in MPC.

When conducting optimization for resilience, most research considers minimizing the total loss-of-load [10], [11], and other resilience metrics like minimum load the system can sustain [11], [12], duration-of-outage [12], percentage of customers experiencing an outage [11] are sometimes adopted for system evaluations. In [13], different values of lost load were used to indicate the priority of load shedding. Here, we consider customers with different values of lost load and penalty function designs toward different resilience metrics for the microgrid scheduling during the contingency period.

II. ELECTROCHEMICAL MODEL OF HYDROGEN STORAGE

In this section, we first describe nonlinear models for electrolyzers and fuel cells [8], [9], and then introduce the piecewise linear approximation model for hydrogen storage.

A. Electrochemical model of electorlyzer

An electrolyzer uses electricity (current) to split water into hydrogen and oxygen. The most widely used type of electrolyzer is the Proton Exchange Membrane (PEM) electrolyzer owing to its fast response time [6, p.5]. We adopt the model for the PEM electrolyzer cells developed by Abomazid et al. in [8], which takes into account the effect of operating temperature, pressure, and the number of identical cells.

Let t be the index for time intervals. We denote the electrolyzer current as $I_t^e(A)$ and the output hydrogen flow rate as $h_t^e(kg/s)$.[2] From Faraday's Law of Electrolysis [6, p.20], the current and hydrogen flow relationship of the electrolyzer is linear, given by

$$h_t^e = k^e n^e I_t^e, \tag{1}$$

where we use a constant coefficient[3] k^e, and n^e is the number of electrolyzer cells connected in series. The input current for the PEM electrolyzer I_t^e and the output power $p_t^e(kW)$ have a nonlinear relationship, given by

$$p_t^e = P_e(I_t^e n^e). \tag{2}$$

Details about this nonlinear function $P_e(\cdot)$ are given in the appendix of our online version [14]. Part of the nonlinearity is caused by the fact that energy is computed by the product of current and voltage. Another part of the nonlinearity comes from the fact that the PEM electrolyzer has nonlinear voltage-current characteristics, resulting from different voltage losses, e.g. activation losses, ohmic losses, and mass transport losses within the cell. The electrochemical kinetics within the cell are described by the Tafel Equation which has logarithmic terms making the polarization curves nonlinear [6, p.29].

Since $P_e(\cdot)$ is a bijective function, we get the following equation explaining the relationship between the input power p_t^e and output hydrogen h_t^e for the PEM electrolyzer by combining equation (2) and (1),

$$h_t^e := f^e(p_t^e) = k^e[P_e]^{-1}(p_t^e). \tag{3}$$

Some papers approximate this nonlinear relationship with $h_t^e \approx (\eta^e p_t^e)/\mathcal{H}$, where $\mathcal{H}$ (kJ/kg) describes the energy content of hydrogen in terms of its higher heating value, and η^e represents a constant efficiency parameter of a PEM electrolyzer, typically lying in the 70-90% range [6, p.4]. However, the performance comparison in our simulation demonstrates the inaccuracy of such a constant efficiency model.

Due to high mass transport losses at high current densities, there is a limit on the maximum allowable current through the cell which thus imposes an upper bound on p_t^e given by

$$0 \leq p_t^e \leq \bar{p}_t^e. \tag{4}$$

B. Electrochemical model of fuel cell

The reverse reaction of using hydrogen to generate power is performed by a PEM fuel cell. The PEM fuel cell (PEMFC) technology is widespread commercially [7]. In this study, we adopted the model from Corrêa et al. which was experimentally validated on a Ballard-Mark-V PEMFC [9].

Similar to the electrolyzer, the linear relationship between the output current $I_t^f(A)$ and input hydrogen $h_t^f(kg/s)$[4] is described by

$$I_t^f = k^f h_t^f / n^f, \tag{5}$$

where n^f represents the number of PEM fuel cells connected in series and k^f is the constant coefficient that converts chemical input to electrical output.

The voltage-current relationships for a single PEMFC follow similar physics as an electrolyzer except that the reactions occuring at the anode and cathode are reversed[5]. This results in a nonlinear relationship between the fuel cell current and power output, $p_t^f(kW)$, given by the function

$$p_t^f = P_f(I_t^f n^f). \tag{6}$$

Details about this nonlinear function $P_f(\cdot)$ formula are explained in the appendix of our online version [14]. Combining (5) and (6) the relationship between the input hydrogen h_t^f and output power p_t^f for PEMFC is given by

$$p_t^f := f^f(h_t^f) = P_f(h_t^f k^f). \tag{7}$$

---

[1]Described by the Ideal Gas Law.
[2]Superscript 'e' represents electrolyzer rather than power of a number.
[3]Detailed expression can be found in [14].

[4]Superscript 'f' represents fuel cell rather than power of a number.
[5]The detailed electrochemical model can be found in the appendix of our online version [14].

Some papers approximate this nonlinear relationship (7) with $p_t^f \approx \eta^f h_t^f \mathcal{H}$. The efficiency η^f of a PEMFC typically lies in the 40-60% [15] range.

The upper bound on the power output of the fuel cell comes from the limit on the current through the cell, *i.e.*,

$$0 \leq p_t^f \leq \bar{p}_t^f. \tag{8}$$

C. Intertemporal relationship of hydrogen storage

The state of hydrogen (SoH) is the mass of hydrogen stored in the hydrogen tank, and it evolves with

$$e_t + (h_t^e - h_t^f)\delta = e_{t+1}, \tag{9a}$$
$$\underline{e} \leq e_t \leq \overline{e}, \quad e_0 = 0.1\overline{e}. \tag{9b}$$

where $e_t(kg)$ is the SoH at time t and δ is the time duration. Expressing SoH in kg allows us to express the intertemporal relationship of the hydrogen storage as (9a) without having to track the operating conditions (e.g. pressure and temperature) of electrolyzers, storage tank, and fuel cells separately. In this study, we assume the initial SoH to be 10% in (9b).

D. Piecewise linear approximation

We approximate the nonlinear electrochemical hydrogen storage model (3) and (7) with piecewise linear functions,*i.e.*,

$$h_t^e = \sum_{k=1}^{K}(a_k^e p_t^e + b_k^e)\mathbb{1}\{p_t^e \in \mathcal{P}_k^e\},$$
$$p_t^f = \sum_{k=1}^{K}(a_k^f h_t^f + b_k^f)\mathbb{1}\{h_t^f \in \mathcal{H}_k^f\}. \tag{10}$$

Here, $\mathcal{P}_k^e$ and $\mathcal{H}_k^f$ represent the k-th pieces for power and hydrogen flow, respectively. The indicator function $\mathbb{1}$ means that $\mathbb{1}\{\mathscr{A}\} = 1$ if $\mathscr{A}$ is true and $\mathbb{1}\{\mathscr{A}\} = 0$ otherwise. The coefficients of each linear piece k are $a_k^e, b_k^e, a_k^f, b_k^f$, which are computed via minimizing the difference between (3),(7), and (10) for the piecewise linear hydrogen storage model.

III. ENERGY MANAGEMENT FOR MICROGRID RESILIENCE

We first introduce the microgrid EMS with green hydrogen storage. Then we explain MPC together with the infeasibility correction method toward grid resilience in real-time.
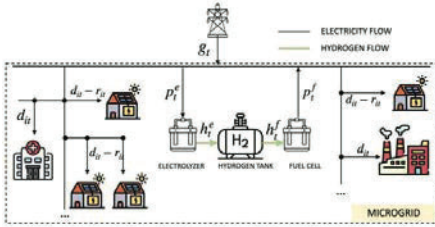
A. A microgrid model

Fig. 1. System schematics for the microgrid with hydrogen storage.

We adopt a simplified system schematic shown in Fig. 1 for the microgrid energy management to enhance resilience with hydrogen storage. At time t, there are two electricity supply sources: the grid energy supply g_t and the roof-top solar r_{it} from household i. Some of this electricity is directly consumed by the household, denoted by d_{it}, while another portion is used to produce hydrogen through electrolyzers, which is subsequently stored in a hydrogen tank. During contingencies, the hydrogen in the tank can be utilized to generate supplementary electricity using fuel cells.

B. Resilence-enhancing microgrid EMS

We considered a microgrid containing customers with different values of the lost load $(v_1, ..., v_N)$. N is the number of households. Critical loads like hospitals have higher values of the lost load. The loss-of-load for customer i at time t is denoted by l_{it}. The electricity price from the grid supply is $c_t \in \mathbb{R}_+$. The objective of EMS is to minimize the penalty induced by the loss-of-load and the cost of purchasing energy from the grid. We consider three types of loss-of-load penalties:

- Type 1 (eg. [10]) adopts l_1-norm $\Phi_i(l_i) = v_i||l_i||_1$ to penalize the total loss-of-load.
- Type 2 (eg. [13]) adopts l_2-norm $\Phi_i(l_i) = v_i||l_i||_2$ to give more penalty for the large value of loss-of-load.
- Type 3 (we propose) adopts a mixed norm of l_1 and l_∞ norms $\Phi_i(l_i) = v_i||l_i||_1 + v_i||l_i||_\infty \cdot T$ to penalize both the total loss-of-load and maximum load shed.[6]

The optimization for microgrid energy management is adopted in the receding horizon for MPC. In each receding horizon from the initial time t' to the end time T, the length of the time horizon is $\mathcal{T} := T - t' + 1$. The roof-top solar generation prediction (r_{it}) and the initial SoH $e_{t'}$ are given. Define $\Omega := \{p^f, p^e, h^f, h^e, e, g \in \mathbb{R}_+^{\mathcal{T}}, D, L \in \mathbb{R}_+^{N \times \mathcal{T}}\}$ for the domain of decision variables, $D := (d_{it})$, and $L := (l_{it})$. The resilience-enhancing microgrid EMS is given by

$$\underset{\Omega}{\text{minimize}} \quad \sum_{i=1}^{N}\Phi_i(l_i) + \sum_{t=t'}^{T}c_t g_t, \tag{11a}$$

subject to $\quad \forall t \in \{t', ..., T\}, \forall i \in \{1, ..., N\}$

$$d_{it} - r_{it} - l_{it} = q_{it}, \tag{11b}$$
$$p_t^f - p_t^e + g_t = \mathbf{1}^\mathsf{T} q_t, \tag{11c}$$
$$\underline{b} \leq A q_t \leq \overline{b}, \tag{11d}$$
$$l_{it} \leq d_{it}, \quad g_t \leq \bar{g}_t, \tag{11e}$$
$$\underline{d}_{it} \leq d_{it} \leq \bar{d}_{it}, \tag{11f}$$
$$(4), (8), (9), (10).$$

For simplicity, we assume each bus only has one customer. In (11b), q_{it} is the net withdraw power of bus i at time t. We have $q_t \in \mathbb{R}^M$ for a M-bus network. In (11c), $\mathbf{1}$ represents a vector of 1's. This constraint means that the storage and outer grid power supply balance the total withdrawal of all buses. We assume the hydrogen storage is connected to the slack bus, the grid connection point in the network. In (11d), we use a linearized DistFlow (LinDistFlow) model for the microgrid network [16]. $A \in \mathbb{R}^{N \times M}$ is the parameter for the LinDistFlow constructed by the network impedance, resistance, and topology information. $\overline{b}, \underline{b}$ are composed of network voltage limits and thermal limits. Details about parameters $A, \overline{b}, \underline{b}$ are in the appendix of [16]. (11e) shows that the customer loss-of-load l_{it} is constrained by the household demand, and the grid supply g_t is constrained by $\bar{g}_t$, the maximum available grid supply. In (11f), $\underline{d}_{it}$ and $\bar{d}_{it}$ are boundary limits on demands.

The piecewise linear approximation (10) of hydrogen storage is adopted in this optimization to substitute nonlinear

---

[6]The first term $||l_i||_1$ is summing $|l_{it}|$ over the entire time horizon, whereas $||l_i||_\infty$ takes only the maximum l_{it} over the time horizon. To increase the contribution of the second term in the mixed norm, we weight it by T.

equality constraints (3) and (7), which will result in a non-convex optimization. Thus, we reduce the computation burden while maintaining an accurate solution. We further formulate (11) into a mixed integer program (MIP) with linear constraints and convex objective (details in [14]).

C. Model predictive control with feasibility projection

The real-time microgrid operation is conducted in a receding window MPC. In both the Type I linear model and the Type II piecewise linear model for storage, the optimal solution might be infeasible under the nonlinear hydrogen storage model. We propose a feasibility projection after finishing the optimization in each receding window. Such a feasibility projection can fix the approximation error in real-time. Here is a high-level summary for the feasibility projection of hydrogen storage operation. If infeasible hydrogen dispatch exceeds the maximum bounds $\overline{e}$, we decrease the electrolyzer output to make SoH bounded by $\overline{e}$; if infeasible SoH is below the minimum bounds $\underline{e}$, we decrease the fuel cell output correspondingly. After achieving a feasible operation for hydrogen storage, we rerun the optimization in that receding window by fixing the hydrogen operation (See detail algorithm in [14]).

IV. NUMERICAL RESULTS

We simulated the microgrid co-operated with hydrogen storage for resilience improvement. The system schematics is shown in Fig. 1. During the contingency caused by an extreme event, the microgrid switched from grid-connected mode to island mode. We conducted simulations comparing three hydrogen storage models with different loss-of-load penalty functions explained in Sec. III-B. (i) The linear model adopted $h_t^e = (\eta^e p_t^e)/\mathcal{H}, p_t^f = \eta^f h_t^f \mathcal{H}$ with $\eta^e = 80\%$ and $\eta^f = 50\%$ for hydrogen storage via receding window MPC. (ii) The proposed piecewise linear storage model was implemented as (11) via receding window MPC. (iii) The nonlinear model (3) and (7) was simulated as an ideal benchmark, which adopted the perfect forecast and solved the dispatch in one shot. The appendix of our online version [14] contains parameters of detailed nonlinear models and additional results.

A. Parameter settings

We simulated a 60-min time horizon with a 40-min island mode contingency for a hypothetical microgrid[7] with 20 households. We considered three categories of customers with different values of lost load[8], *i.e.*, type-1 $v_1 = \$5/\text{kWh}$, type-2 $v_2 = \$1/\text{kWh}$, and type-3 $v_3 = \$0.5/\text{kWh}$. There were 5,7, and 8 customers in each of these categories. Demand lower bounds $\underline{d}$ were set to be 13, 10, and 8 kW respectively for the three categories. We set $c_t = \$0.1/\text{kW}, \forall t$ for the outer grid electricity price, the maximum hydrogen storage charge and discharge rates 150 kW ($\bar{p}^e$) and 70 kW ($\bar{p}^f$), the storage tank capacity ranged from 0 to 3 kg ($\underline{e}$ and $\overline{e}$), the higher heating value of hydrogen $142 MJ/kg$ ($\mathcal{H}$).

To simulate the 40-min island mode contingency, the maximum grid supply capacity $\bar{g}_t$ was 0 kW (*i.e.,* complete outage) for $t \in \{11, .., 40\}$, and 1000 kW for other intervals. We used

Pecan Street data[9] for household consumption and rooftop solar generation. Solar forecasts r_{it}, took the mean data from 7 PM - 8 PM with Gaussian noise, $\mathcal{N}(0, 1)$ kW, added.

B. Performance evaluation

A resilient microgrid anticipates small total loss-of-load and large minimum system load[10] the microgrid can sustain during the contingency. We define the dominated area for one marker as its top-left area in Fig. 2 because points in the dominated area perform worse than the markers for both resilience metrics.
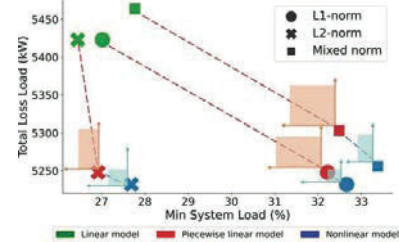

Fig. 2. Total loss-of-load of the microgrid and the minimum system load sustained. (Top left of each marker is the dominated area.)

Our observations for these two resilience metrics in Fig. 2 are three-fold. First, the linear model is always dominated by the piecewise linear model, because the green markers always fall into the dominated area of the red markers under different penalty functions. Second, the piecewise linear model approaches the nonlinear model, the ideal benchmark, from which the linear model is far away. This is represented by the length of dash curves in Fig. 2, and we observe that the red curves are longer than the blue. Third, comparing different penalty functions, the l_1-norm penalty (circular markers) consistently results in the lowest total loss-of-load, attributed to the direct penalization for this metric; the mixed-norm penalty (square markers) outperforms in the minimum system load due to its l_∞-norm penalizing extreme load-shedding.

TABLE I
SYSTEM COST

Penalty	Linear		Piecewise Linear		Nonlinear	
	Cost	% +/-	Cost	% +/-	Cost	% +/-
l_1-norm	$5127	+17%	$4415	+0.8%	$4377	-
l_2-norm	$5956	+6.4%	$5614	+0.3%	$5596	-
Mixed norm	$5361	+21.7%	$4448	+0.9%	$4404	-

System costs, which include the value of lost load and the cost of grid energy supply (computed by $\sum_{t=0}^{T-1}(v_i l_{it} + c_t g_t)$) are shown in Table I. The costs of linear and piecewise linear storage models are expressed as a percentage increase/decrease relative to the cost of the ideal nonlinear benchmark in the column "% +/-". Two key observations emerge. First, there exists a less than 1% disparity in cost between the piecewise linear and nonlinear models. In contrast, the linear model results in a 6.4%-21.7% increase in cost compared to the benchmark. Second, the lowest cost is attained with the l_1-norm penalty, given its direct minimization within the objective function.

The metrics pertaining to time, i.e. the duration-of-outage (DO) as a percentage of the 60-min time horizon and the

---

[7]The network constraints were set to be unbinding for the microgrid, equivalent to a single bus system.

[8]Values of lost load and pricing parameters were set based on [17].

[9]The data is accessible at Pecan St. Project.

[10]This refers to the minimum of the resilience trapezoid in Fig. 3, If the maximum loss-of-load increases, then the minimum system load % decreases.

TABLE II
TIME METRICS FOR TYPE-2 CUSTOMERS

Penalty	Linear		Piecewise Linear		Nonlinear	
	DO	BTO	DO	BTO	DO	BTO
l_1-norm	51.67%	11	38.34%	22	38.34%	22
l_2-norm	23.34%	21	20%	31	5%	41
Mixed norm	50%	11	26.67%	21	-	-

beginning time of outage (BTO), which corresponds to the time (in min) at which the system load percentage first goes below 1% in Fig. 3 (second row) are tabulated in Table II[11]. Note that for the DO we consider the total time for which system load percentage is below 1%. From the data presented in Table II, two key observations emerge. First, as seen for all the other metrics, the linear model deviates significantly in performance from the ideal benchmark. On the other hand, the piecewise linear model closely approximates the ideal benchmark. Specifically, in comparison to the linear model, the piecewise linear model reduces the DO by 13%-48%. Second, when subject to the l_2-norm penalty, DO is reduced, and BTO is delayed, signifying that the outage takes place later in the 60-min time horizon. This pattern is consistent across all three storage models. We observe a 54.7% reduction in DO for the linear model, while a rather significant 87% reduction for the nonlinear model. The BTO is delayed by 41%-91% under the l_2-norm penalty.[12]
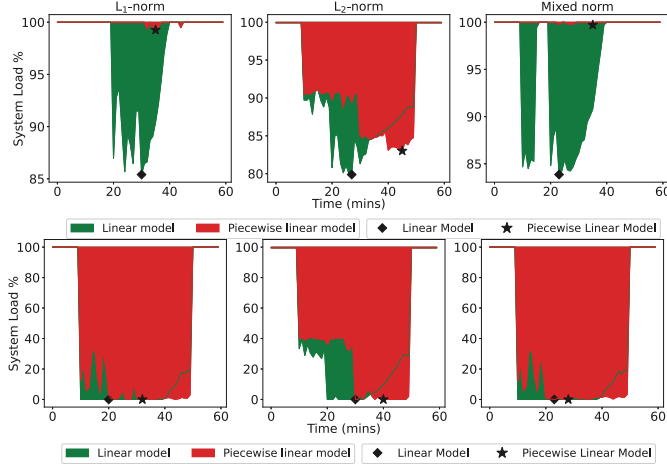

Fig. 3. Top to Bottom: Resilience trapezoids for type-1 customers and type-2 customers. Left to Right: Resilience trapezoids under different penalty schemes (The diamond and star markers represent the minimum points).

In Fig. 3, we depict resilience trapezoids with total system load percentage, which is the load demand excluding loss-of-load as a percent of the total demand on the Y-axis. The "resilience trapezoid" [12] provides a visualization of the system states. The shaded area represents the total loss-of-load percentage and the markers represent the minimum system load percentage. Comparing the linear and piecewise linear models we observe: (i) For type-1 customers (Fig. 3 first row), the piecewise linear model reduces total loss-of-load by 95% under the l_1 and mixed-norm penalties and 12% under the l_2-norm compared to the linear storage model; (ii) For type-2 customers (Fig. 3 second row), reductions of 6% under the l_2-norm and 2% under the l_1-norm are observed.

[11]'-' implies there is no outage in Table II.
[12]See [14] for more simulations exploring this phenomenon.

V. CONCLUSIONS

To improve electricity supply resilience, we co-optimize microgrid and hydrogen storage operation with the proposed piecewise linearization model, capturing the nonlinear electrochemical model of electrolyzers and fuel cells. This approach implemented with a feasibility projection method in model predictive control accurately approximates the performance of the ideal nonlinear benchmark model for hydrogen storage. Besides, this paper has limitations in considering only operations during the contingency. In our future work, we will explore joint optimization for both pre-contingency and during-contingency operations.

REFERENCES

[1] Y. Zhang, P. E. Campana, A. Lundblad, and J. Yan, "Comparative study of hydrogen storage and battery storage in grid connected photovoltaic system: Storage sizing and rule-based operation," *Applied energy*, vol. 201, pp. 397–411, 2017.

[2] J. Tobajas, F. Garcia-Torres, P. Roncero-Sánchez, J. Vázquez, L. Bellatreche, and E. Nieto, "Resilience-oriented schedule of microgrids with hybrid energy storage system using model predictive control," *Applied Energy*, vol. 306, p. 118092, 2022.

[3] H. Haggi, W. Sun, J. M. Fenton, and P. Brooker, "Proactive rolling-horizon-based scheduling of hydrogen systems for resilient power grids," *IEEE Transactions on Industry Applications*, vol. 58, no. 2, pp. 1737–1746, 2022.

[4] P. Gabrielli, B. Flamm, A. Eichler, M. Gazzani, J. Lygeros, and M. Mazzotti, "Modeling for optimal operation of pem fuel cells and electrolyzers," in *2016 IEEE 16th International Conference on Environment and Electrical Engineering (EEEIC)*, 2016, pp. 1–7.

[5] B. Flamm, C. Peter, F. N. Büchi, and J. Lygeros, "Electrolyzer modeling and real-time control for optimized production of hydrogen gas," *Applied Energy*, vol. 281, p. 116031, 2021. [Online]. Available: https://www.sciencedirect.com/science/article/pii/S0306261920314690

[6] D. Bessarabov, H. Wang, H. Li, and N. Zhao, *PEM electrolysis for hydrogen production: principles and applications*. CRC press, 2016.

[7] J. Larminie, A. Dicks, and M. S. McDonald, *Fuel cell systems explained*. J. Wiley Chichester, UK, 2003, vol. 2.

[8] A. M. Abomazid, N. A. El-Taweel, and H. E. Farag, "Novel analytical approach for parameters identification of PEM electrolyzer," *IEEE Transactions on Industrial Informatics*, vol. 18, no. 9, pp. 5870–5881, 2021.

[9] J. M. Corrêa, F. A. Farret, L. N. Canha, and M. G. Simoes, "An electrochemical-based fuel-cell model suitable for electrical engineering automation approach," *IEEE Transactions on industrial electronics*, vol. 51, no. 5, pp. 1103–1112, 2004.

[10] Y. Yao, W. Liu, R. Jain, B. Chowdhury, J. Wang, and R. Cox, "Quantitative metrics for grid resilience evaluation and optimization," *IEEE Transactions on Sustainable Energy*, vol. 14, no. 2, pp. 1244–1258, 2022.

[11] C. Nan and G. Sansavini, "A quantitative method for assessing resilience of interdependent infrastructures," *Reliability Engineering & System Safety*, vol. 157, pp. 35–53, 2017. [Online]. Available: https://www.sciencedirect.com/science/article/pii/S095183201630374X

[12] M. Panteli, P. Mancarella, D. N. Trakas, E. Kyriakides, and N. D. Hatziargyriou, "Metrics and quantification of operational and infrastructure resilience in power systems," *IEEE Transactions on Power Systems*, vol. 32, no. 6, pp. 4732–4742, 2017.

[13] A. Hussain, V.-H. Bui, and H.-M. Kim, "Resilience-oriented optimal operation of networked hybrid microgrids," *IEEE Transactions on Smart Grid*, vol. 10, no. 1, pp. 204–215, 2017.

[14] S. Dhankar, C. Chen, and L. Tong, "Enhancing microgrid resilience with green hydrogen storage," *arXiv preprint arXiv:2311.13149*, 2023.

[15] E. Eriksson and E. M. Gray, "Optimization and integration of hybrid renewable energy hydrogen fuel cell energy systems–a critical review," *Applied energy*, vol. 202, pp. 348–364, 2017.

[16] C. Chen, S. Bose, M. Timothy, and L. Tong, "Wholesale market participation of dera: DSO-DERA-ISO coordination," *arXiv preprint arXiv:2307.01999*, 2024.

[17] "ERCOT staff recommendation to committee," [ONLINE], available at https://www.ercot.com/files/docs/2023/04/11/10.1%20Phase%202 0%20Market%20Redesign%20-%20Bridging%20Solutions.pdf, April 2023.